PAPER • **OPEN ACCESS**

Morphological control of seedlessly-synthesized gold nanorods using binary surfactants

To cite this article: Lucien Roach *et al* 2018 *Nanotechnology* **29** 135601

OPEN ACCESS
IOP Publishing
Nanotechnology

Nanotechnology **29** (2018) 135601 (8pp)
https://doi.org/10.1088/1361-6528/aaa99d

Morphological control of seedlessly-synthesized gold nanorods using binary surfactants

Lucien Roach[1,2], Sunjie Ye[1,2], Samuel C T Moorcroft[1], Kevin Critchley[1], P Louise Coletta[2] and Stephen D Evans[1,2]

[1] School of Physics and Astronomy, University of Leeds, Leeds, LS2 9JT, United Kingdom
[2] Leeds Institute for Biomedical and Clinical Sciences, University of Leeds, Leeds, LS9 7TF, United Kingdom

E-mail: s.d.evans@leeds.ac.uk

Received 8 December 2017, revised 17 January 2018
Accepted for publication 22 January 2018
Published 13 February 2018

Abstract

High purity gold nanorods (AuNRs) with tunable morphology have been synthesized through a binary-surfactant seedless method, which enables the formation of monocrystalline AuNRs with diameters between 7 and 35 nm. The protocol has high shape yield and monodispersity, demonstrating good reproducibility and scalability allowing synthesis of batches 0.5 l in volume. Morphological control has been achieved through the adjustment of the molar concentrations of cetyltrimethylammonium bromide and sodium oleate in the growth solution, providing fine tuning of the optical scattering and absorbance properties of the AuNRs across the visible and NIR spectrum. Sodium oleate was found to provide greatest control over the aspect ratio (and hence optical properties) with concentration changes between 10 and 23 mM leading to variation in the aspect ratio between 2.8 and 4.8. Changes in the geometry of the end-caps were also observed as a result of manipulating the two surfactant concentrations.

Supplementary material for this article is available online

Keywords: morphological control, gold nanorod, binary surfactant, one-pot synthesis, high purity

(Some figures may appear in colour only in the online journal)

1. Introduction

The use of gold nanoparticles (AuNPs) as potential photothermal conversion agents for use in diagnostic imaging and therapy (theranostics) has been a recent area of interest [1–4]. Their tunable optical properties, easily modified surface chemistry and high light-to-heat conversion efficiency have made them appealing as vehicles for photoacoustics and photothermal therapy [5–7]. Many AuNPs exhibit strong optical absorbance in the near-infrared biological window, a range of wavelengths in which human tissue exhibits enhanced light penetration up to several centimetres, enabling their use as *in vivo* theranostic agents [7]. NIR absorbing AuNP morphologies such as nanorods [8, 9], nanoshells [10, 11], nanotubes [12] and nanocages [13] have all become areas of active research.

Gold nanorods (AuNRs) have attracted particular attention because of the strong narrow absorbance band associated with their longitudinal surface plasmon resonance (LSPR) mode, the peak wavelength of which is tunable through modification of the AuNR aspect ratio [14, 15]. Typically, AuNRs exhibit larger molar extinction coefficients, of around $\sim 10^{10}$ M^{-1} cm^{-1} [16], more than double that expected from gold nanoshells [17]. This gives higher light absorption compared with other AuNP morphologies allowing greater heat generation [18]. Consequently AuNRs have been demonstrated as suitable contrast

agents in photoacoustic imaging [19, 20]. They have also been shown to be effective at killing cancerous cells *in vitro* under NIR illumination [21] and have been used to ablate tumors *in vivo* as photothermal conversion agents in plasmonic photothermal therapy [22, 23]. For thicker AuNRs, the accompanying light scattering properties has also made them appealing for use as biosensors [24].

In order to translate these approaches to the clinic, the need for synthesis protocols which yield high quality AuNRs on large scales, in a simple, reliable and scalable process continues to grow in importance. Aqueous-phase syntheses first appeared in 2001, as a two-step process based on the formation of seed particles and the subsequent reduction of gold onto these in a strong surfactant solution to yield rod-like particles [25]. However, these protocols have shown problems with reproducibility, largely due to the difficulty in attaining the stable penta-twinned seeds required for rod formation in high yield [26]. Despite recent progress in improving the yield of twinned-seeds through thermal annealing [27], methods that forego the seed-synthesis step all together remain attractive. The first seedless AuNR synthesis was developed in 2005 by Jana *et al* [28], allowing the formation of AuNRs in a one-pot protocol. Whilst these syntheses are more straightforward to perform than traditional seeded protocols, they have historically suffered from higher polydispersity, lower shape yield, and have been restricted to smaller diameters (typically ∼10 nm).

Seedless protocols have improved significantly since their inception, with improved monodispersity following the optimization of the growth pH [29]. Other advancements have followed alongside changes seen in seeded growth protocols where the inclusion of aromatic additives [30–34] and modification of the surfactants used during the growth [35–38], have led to significantly improved monodispersity and morphological control of the final product, in particular the inclusion of sodium oleate [39]. Lai *et al* have subsequently demonstrated similar improvements in seedless protocols through the addition of sodium oleate, increasing the range of achievable diameters up to 37 nm, with significantly improved shape yield and monodispersity [40]. They also further modified the morphology of the final AuNRs through control of the $AgNO_3$ and $NaBH_4$ concentrations in the growth solution, controlling this through underpotential deposition and the number of nucleation sites respectively.

Here we investigate the effects of simultaneously modifying the concentrations of sodium oleate and cetyltrimethylammonium bromide (CTAB) in a one-pot binary surfactant synthesis protocol, which offers simplified route for controlling the morphology of seedlessly-synthesized AuNRs through direct manipulation of the soft-template. We have explored an effective and reproducible method to precisely control the geometry of AuNRs, allowing diameters between 7 and 35 nm, and LSPR wavelengths ranging from 620 to 900 nm to be realized. Samples were produced with AuNR yields nearing 100% and negligible shape impurities, thus requiring no post-purification of the AuNR solutions.

2. Experimental section

2.1. Materials

Gold (III) chloride trihydrate (520918), hexadecyltrimethylammonium bromide (H6269), and sulphuric acid (07208) were purchased from Sigma-Aldrich. L-(+)-ascorbic acid (A15613) was purchased from Alfa Aesar. Silver nitrate (11414), sodium borohydride (10599010), hydrochloric acid (11.7 M, UN1789), nitric acid (70%, UN2031), ethanol (E/0650DF/17), and hydrogen peroxide (H/1750/17) were purchased from Fisher Scientific. Sodium oleate (O0057) was purchased from TCI. 2-propanol (20842) and acetone (20066) were ordered from VWR. Milli-Q water (18 MΩ cm) was used in the preparation of all solutions. All chemicals were used without further purification.

2.2. Synthesis of AuNRs

20 ml borosilicate glass vials were cleaned with *aqua regia* (1:3 mix of nitric and hydrochloric acid) for 30 min, thoroughly rinsed with Milli-Q water and stored in an oven at 80 °C oven before use. Once dry the vials were cooled to 30 °C, and maintained at this temperature during the synthesis. Solutions of CTAB and sodium oleate (200 mM) were prepared in advance of the synthesis heated to 70 °C until all the solute was dissolved. These were then added in the desired ratio and topped up to 5 ml with Milli-Q (total surfactant concentration between 20 and 180 mM). This was followed by the sequential addition of 5 ml $HAuCl_4$ (1 mM), 240 μl $AgNO_3$ (4 mM), 50 μl HCl (11.7 M), and 75 μl ascorbic acid (85.8 mM). To this 7.5 μl freshly prepared, ice-cold $NaBH_4$ (10 mM) was rapidly injected into the mixture. The mixture was then kept at 30 °C for 4 h. The AuNRs were then isolated by centrifugation at 9000 g for 30 min. The supernatant was discarded and the precipitate resuspended in Milli-Q. AuNR solutions were stored in the dark at room temperature.

This method has been scaled up to larger batch sizes of ∼0.5 l with some modification. The initial CTAB-oleate surfactant mix was prepared by heating 250 ml Milli-Q water to 70 °C in a water bath, under constant stirring. The desired quantity of CTAB and sodium oleate were then added directly to the heated water and stirred until completely dissolved. The stirred solution was then cooled to 30 °C. 6 ml $AgNO_3$ (4 mM), 2.5 ml HCl (12 M), 250 ml $HAuCl_4$ (1 mM), 3.75 ml ascorbic acid (85.8 mM) added in sequence under constant stirring, the mixture was allowed to stir for ∼5 min between addition of each solution. Finally, the stirring of the solution was increased to 1200 rpm and 0.375 ml ice-cold freshly-prepared $NaBH_4$ (10 mM) was rapidly injected. Stirring was immediately ceased and the solution kept at 30 °C for 4 h. The resulting AuNRs were cleaned by centrifugation at 9000 g for 30 min as above.

2.3. Characterization

UV–vis absorption spectra were taken on AuNR solutions diluted by a factor of 10 from the as-synthesized solution using a Perkin-Elmer Lambda 35 spectrophotometer. Lower magnification TEM

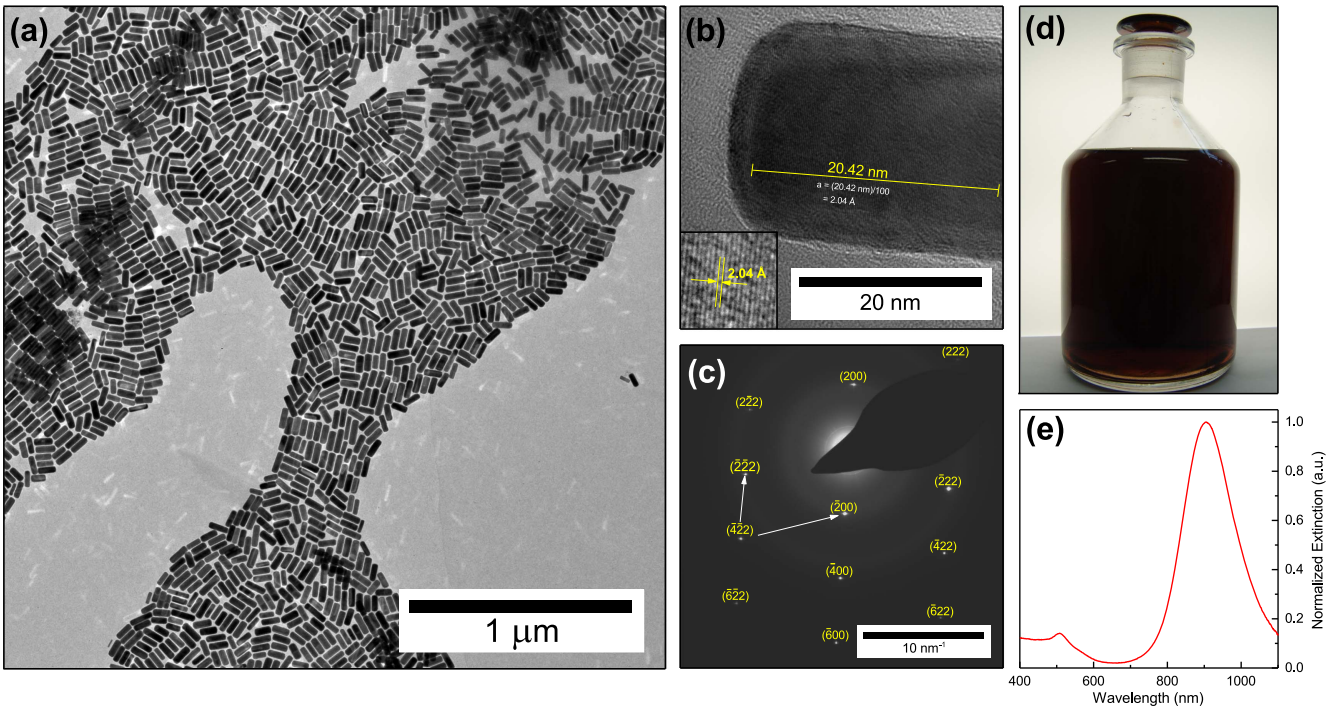

Figure 1. (a): Wide-field TEM image of sample showing good monodispersity and high shape yield. (b): High resolution TEM showing the crystalline structure of a AuNR synthesized using a 48 mM CTAB—15 mM oleate growth solution. Annotated on the image is the measured lattice spacing of 2.04 Å (calculated from 100 lattice rows), corresponding to a (200) lattice spacing. Inset is a (4 × 4) nm region showing the visible lattice structure. (c): Selected area electron diffraction image of the same AuNR. The corresponding Miller indices for each spot have been labeled on the figure. These are consistent with a monocrystalline FCC metal. (d): Photo of a 500 ml as-synthesized AuNR batch synthesized using a 60 mM CTAB—12.5 mM oleate growth solution (e): UV–vis spectrum of the same 500 ml solution normalized to peak extinction.

images were obtained using a Tecnai G2 Spirit TWIN/BioTWIN with an acceleration voltage of 120 kV. A field emission gun TEM microscope (Philips CM200 FEGTEM; 200 kV) equipped with a Gatan GIF200 imaging filter running Digital-Micrograph software was used to take higher magnification TEM and selected area of diffraction images. TEM samples were prepared by drying ~5 μl of 10× concentrated nanoparticle dispersion (in Milli-Q) on an amorphous carbon-coated 400-mesh copper grid (Electron Microscopy Services, CF400-Cu). Sizes of AuNRs were measured manually using ImageJ. Zeta potential measurements were taken using a Malvern Zetasizer-Nano Series-Zen 3600. A Varian 240 fs atomic absorbance spectrometer was used to ascertain the concentration of Au^0 in AuNR solutions. This was used in conjunction with the TEM determined geometries to ascertain the concentration of particles in solution.

2.4. Darkfield microscopy and single particle spectroscopy

Darkfield microscopy images were taken on a Nikon Ti–S microscope using a TI-DF dry darkfield condenser and a CFI Plan Fluor 100× oil-coupled objective. Images were captured using an Olympus UC90 camera and spectra collected via Ocean Optics QE-Pro fiber-coupled to the microscope with a 1000 μm fiber optic (Ocean Optics, QP1000-2-VIS-BX). The fiber optic collected light from a 10 μm spot. In order to obtain a scatter spectrum, background spectra were collected from regions without particles. A particle was then moved into the central focus and a spectrum collected. The background spectrum was then subtracted from this and then divided through by the normalized illumination spectrum, to correct for the non-uniform power spectrum density of the bulb. Particles with a LSPR outside of the human visual spectrum (>750 nm) were beyond the spectral range of the camera. The following steps during sample preparation were found to minimize background scatter during spectra collection. Samples were prepared on (24 × 50) mm coverslips (Menzel Gläser, CS2450100). To minimize background scatter these cleaned by washing sequentially in 10% Decon90 solution, acetone, isopropanol and finally Milli-Q water. These were then placed in piranha solution (3:1 mix of sulphuric acid and hydrogen peroxide) heated to 80 °C for 30 min, rinsed using Milli-Q and then stored under ethanol until use. After drying, the coverslip was placed in a spin-coater and 100 μl of AuNR solution diluted to ~5 pM was placed onto the center of it. The coverslip was spun at 1000 rpm for 1 min ensuring all particles which adhered to the surface were well separated during imaging and spectra collection.

3. Results and discussion

3.1. Synthesis and morphological control of AuNRs

AuNRs were synthesized using a binary-surfactant seedless protocol similar to that published by Lai *et al* [40], but

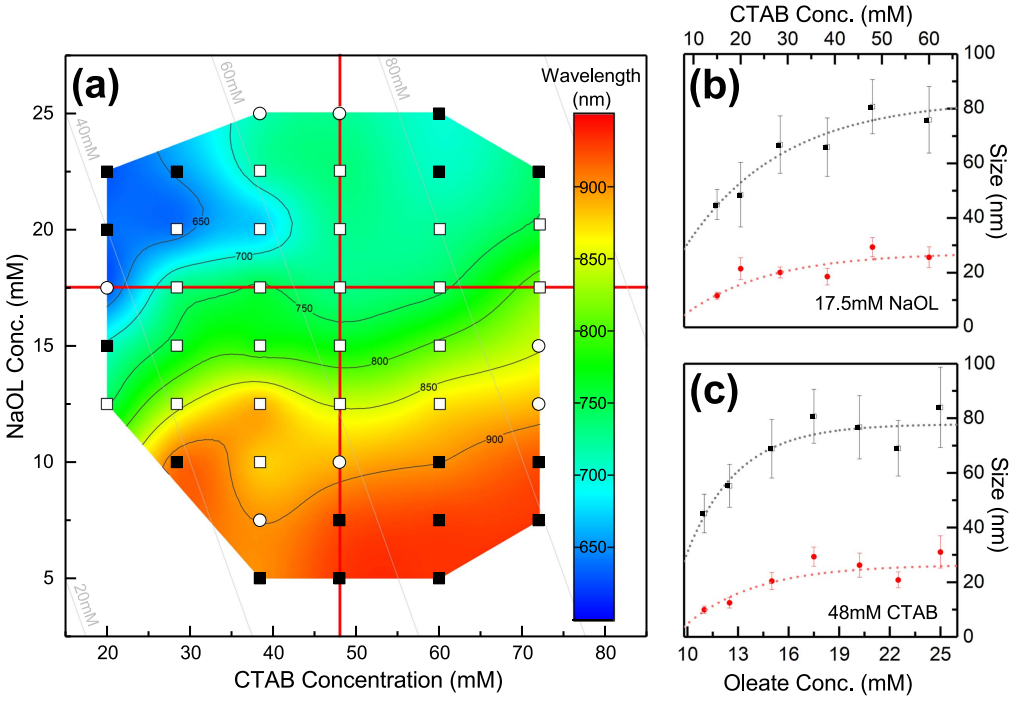

Figure 2. (a): Effect of surfactant concentration on LSPR wavelength with all other components held constant. Batches of AuNRs were prepared at CTAB and sodium oleate concentrations indicated by a point. The shape of the points indicate yield, with: □ > 98% AuNRs; ○ > 90% AuNRs; ■ — low shape yield. The LSPR wavelength is interpolated between point, the color scale for this is given in the right of the figure. (b): Effect of CTAB concentration on length (black) and diameter (red) of AuNRs at a constant oleate concentration of 17.5 mM (horizontal line in (a)). (c): Effect of oleate concentration on length (black) and diameter (red) of AuNRs at a constant CTAB concentration of 48 mM (vertical line in (a)). Error bars indicate the standard deviation of the AuNRs in each batch.

extended the range of surfactant concentrations used to control the morphology. The particles were formed in a growth solution containing a mixture of CTAB and sodium oleate in the presence of a weak reducing agent, ascorbic acid, and silver nitrate. After addition of the $HAuCl_4$ solution, the mixture turned a dark orange–yellow as the $[AuCl_4]^-$ formed a complex with $[CTA]^+$ ions in solution [41]. The unsaturated double-bond of sodium oleate is capable of reducing Au^{3+} to Au^{1+}, as indicated by the clearing of the mixture [39, 40]. To this $AgNO_3$, HCl and ascorbic acid were added sequentially. High-yield synthesis of AuNRs was only possible at a low pH of ~1.5 [29], which was achieved through increasing the volume of HCl added to the growth mixture. Any remaining yellow in the solution cleared following the addition of ascorbic acid. Finally, nucleation of the particles was initiated by the rapid injection of freshly prepared ice-cold $NaBH_4$. The solution was then left unstirred for 4 h, at 30 °C. Particles were then cleaned by centrifugation at 9000 g. The supernatant was discarded and the precipitate resuspended in Milli-Q water.

This protocol showed good reproducibility, with little variation in optical properties between different batches grown to the same recipe (see figure S2 is available online at stacks.iop.org/NANO/29/135601/mmedia) and can be scaled up substantially (e.g. 500 ml) with only a minor reduction in the quality of the end product (figures 1(d) and (e)). The samples synthesized by this protocol showed very high shape yields, normally in excess of 98% as shown in figure 1(a). For several batches it was not possible to locate any non-rodlike AuNPs, indicative of 100% yield. Consistent with other seedless protocols the synthesized AuNRs are monocrystalline, as indicated by the strong diffraction pattern seen using SAED (figures 1(b) and (c)).

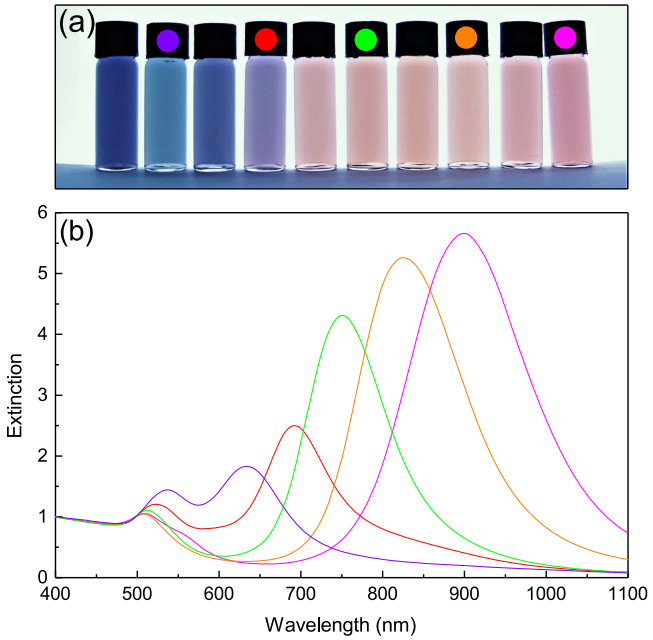

Figure 3. (a): Photograph of particle solutions exhibiting LSPR from 520 to 900 nm, colored circles on lid indicate the associated UV–vis spectrum shown in (b). (b): UV–vis spectra of solutions with resonances over same range. Spectra have been normalized to unity at 400 nm [41].

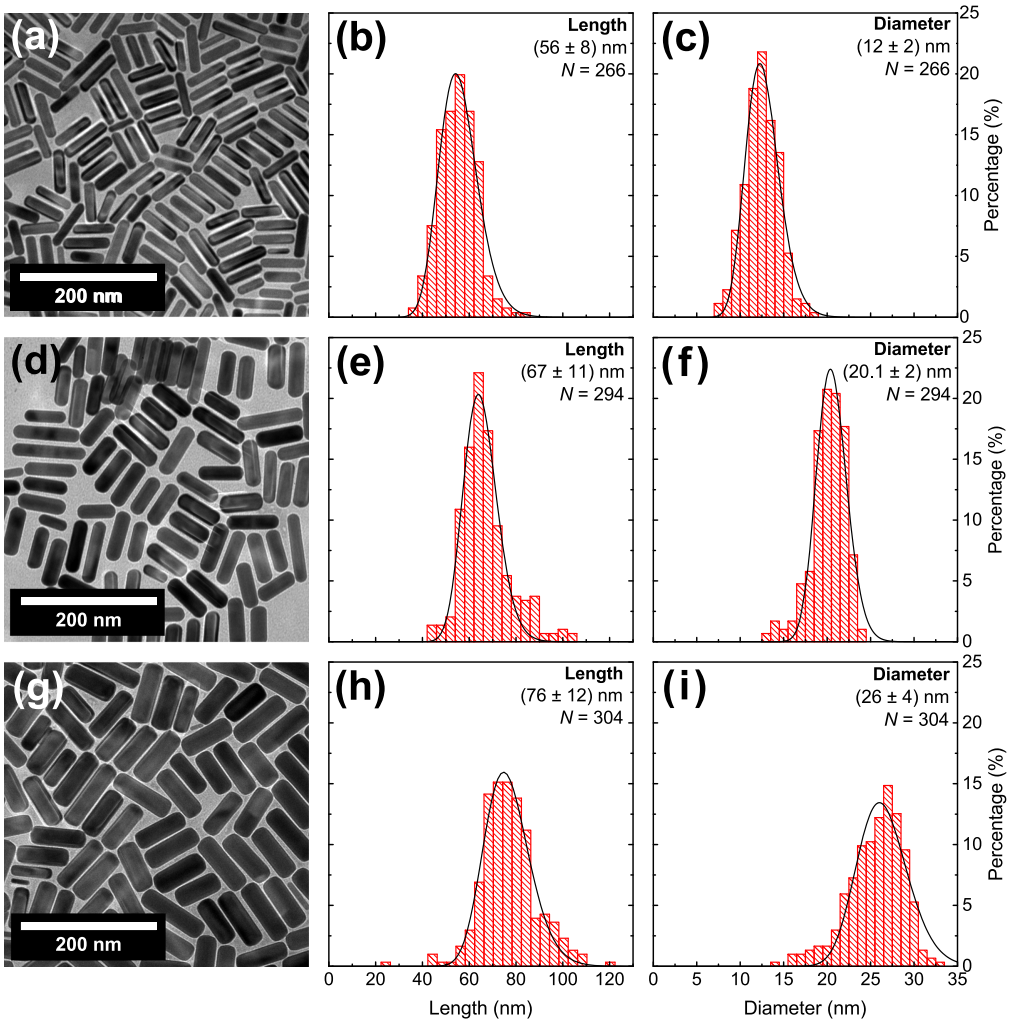

Figure 4. TEM images alongside associated size distributions for the lengths and diameters of selected particles showing the difference in particle morphology at three different pairs of surfactant concentrations. (a)–(c): AuNRs synthesized in a 48:12 CTAB:oleate growth solution (conc. in mM). (d)–(f): (28:17.5) growth solution. (g)–(i): (60:20.2) growth solution. All particle dimensions were determined by analysis of TEM images, sizes are given as $(\bar{x} \pm \sigma_x)$ nm and fitted using a log-normal distribution.

It was found that the morphology of AuNRs could be directly modified through variation of the concentrations of both oleate and CTAB in the growth solution. Holding all other parameters constant a range of viable surfactant concentrations emerged which yielded the seedless synthesis of AuNRs with good shape yield as shown in figure 2(a). These were broadly within concentrations of CTAB between 22 and 70 mM, and sodium oleate between 10 and 23 mM, outside of which the shape yield reduced rapidly, noticeable through the appearance of a third peak at 530 nm due to the presence of spherical inclusions. Within this region batches with high shape purity were synthesized with LSPR values between 620 and 890 nm (figure 3). There is a much greater change in aspect ratio gained through variation of the oleate concentration compared to varying that of CTAB (figures 2(b) and (c)). The LSPR was seen to decrease with increasing oleate concentration, indicating a reduction in aspect ratio. TEM images of the particles showed that this occurred through an increase in the diameter of the synthesized AuNRs whilst yielding a proportionally smaller increase in the length blue-shifting the LSPR (figures 4(a)–(i)). By contrast, a much greater change in the concentration of CTAB was required to have similar effects on the geometry of particles. Potentially the increased range of sizes made available here could be extended further through direct overgrowth in a two-step process [42]. Size distributions and TEM images are available in the supplementary information (sections S1 and S2).

There is also a noticeable difference in the end-cap morphology of the AuNRs alongside the changes in the overall morphology of the AuNRs. With some batches showing end-caps varying in shape between hemispheres and flattened near-cylindrical tips (section S2). Tip geometry is known to change the optical properties of AuNRs, red-shifting the LSPR with decreasing tip eccentricity [43, 44], hence control of this represents a route for further modifying the optical properties of synthesized AuNRs. It is also expected to be of importance in the packing of AuNR assemblies, with flatter caps exhibiting higher capillary forces due to the increased available contact surface [45],

making tip-to-tip arrangements more energetically favorable. Comparison with simulated spectra of AuNRs of varying tip morphology show that the measured resonances fall within the ranges expected from theoretical predictions (figure S5). However, there is some deviation between the simulations and the experimental data, especially for the hemispherically-capped samples, which showed generally higher resonances than expected. Hence this synthesis protocol affords some control over the end-cap morphology of seedlessly-synthesized AuNRs.

For surfactant concentrations which demonstrated a low shape yield, it was found that decreasing the pH further significantly improved the shape yield [29], although this was accompanied by a corresponding red-shift of the LSPR (figure S3) [46]. It seems likely the range of currently viable recipes, may be extended through further optimization of the concentrations of other components in the system. The samples synthesized by this protocol displayed good monodispersity, as indicated by the well-defined LSPR mode in the UV–vis spectra and confirmed by TEM images for a number of samples. Typically the standard deviation of a sample amounted to approximately ∼15% of both the diameter and length (section S1). The well defined NIR absorbance peaks resulting from this low polydispersity will make them well-suited for use as contrast agents in photoacoustic imaging [7]. The strong narrow absorbance bands will provide more efficient heat generation for plasmonic photothermal therapies [47].

The interaction between two surfactants in the system allows the synthesis of a much wider range of AuNR sizes with higher shape purity. It is known that the addition of a negatively-charged oleate ion to the micellular CTAB structure screens electrostatic repulsion between the head groups allowing denser packing of the surfactant monomers leading to preferential formation of rod-like micelles at reduced surfactant concentrations [48]. This is evident in studies of micelle formation in CTAB-oleate mixtures which show a significant reduction in the 2nd critical micelle concentration (CMC) and free energy of rod-like micellisation, compared with those for pure CTAB solutions [49, 50]. The 2nd CMC is reduced from 37 mM for 100% CTAB solutions [51] to ∼1 mM for 90% CTAB—10% oleate mixtures [49, 50]. This appears to be crucial in controlling the formation of AuNRs at lower surfactant concentrations. We have synthesized AuNRs with high yield at CTAB concentrations as low as 20 mM, by contrast without the presence of oleate, concentrations of CTAB in excess of 100 mM were required, well above the 2nd CMC are typically required [28, 29]. It seems likely that the increased packing of surfactant monomers in binary surfactant systems is crucial to accessing larger AuNRs, as it leads to a reduction in the flexibility of the micellular template and hence increased radius of curvature, whilst simultaneously making the synthesis of rod-shaped particles more energetically preferable [52].

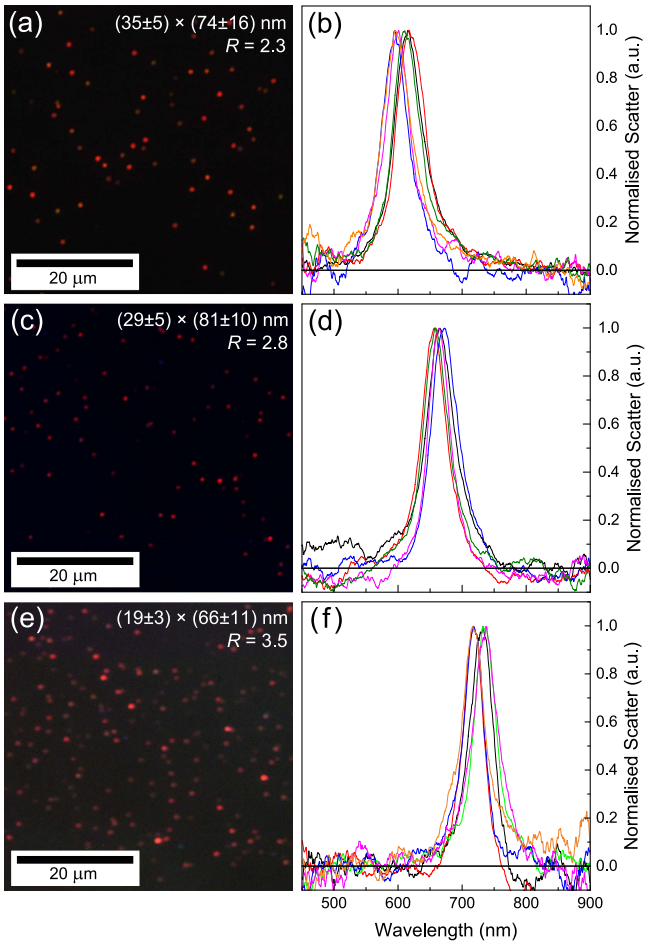

Figure 5. Darkfield microscopy images of AuNRs of different aspect ratio (*R*) spun-coat on a glass surface, average particle dimensions are inset on each figure. Alongside single particle spectra obtained for each sample, showing the expected red-shift with increasing aspect ratio. (a) and (b): (35 ± 5) × (74 ± 16) nm AuNRs. (c) and (d): (29 ± 5) × (81 ± 10) nm AuNRs. (e) and (f): (19 ± 3) × (66 ± 11) nm AuNRs. Darkfield images are given at optimum exposure and gain settings for each sample. Particle sizes and standard deviations are taken from TEM measurements (section S1).

3.2. Darkfield microscopy and single particle spectroscopy

To investigate the change in the optical properties of the AuNRs at the single particle level, darkfield microscopy was performed on several batches of AuNRs. Diluted AuNR solutions were spin-coated on a glass cover-slip to provide well separated individual scatterers suitable for single particle spectroscopy. It was found that AuNRs with diameters below 15 nm were beneath the detection threshold of the single particle spectroscopy system, due to the drop-off in scattering cross section with the square of the AuNP volume (as approximated by Gans theory) [53]. Images showed sharp individual spots with a consistent color demonstrating the AuNPs were well separated on the substrate and monodisperse (5(a)–(c)). Particles appeared red in color as expected for AuNRs with resonances in the NIR [21]. Recorded single particle spectra showed distinct sharp resonance peaks for every AuNR measured, red-shifting with increasing average

aspect-ratio (figures 5(d) and (e)). The signal-to-noise ratio of the LSPR mode is noticeably improved for thicker AuNRs, in agreement with Gans theory [53]. The observed peaks show close agreement with the optical properties expected at the morphologies given based on finite-element simulations of their properties (figure S4).

4. Conclusion

We have demonstrated that manipulation of the concentrations of CTAB and sodium oleate in the seedless synthesis of AuNRs represents a reliable method for the controlled modification of the morphology of AuNRs. The protocol has been shown to yield seedlessly-synthesized AuNRs of tunable dimensions with high shape yield and good monodispersity in a scalable manner. It has also showed potential as a method for providing more control over AuNR end-cap morphology. The improvements obtained through the modification of the soft template may serve as a further basis for continued advances in the controlled synthesized of one-dimensional nanostructures. This simple and cost-effect method affording control of optical properties will be of direct benefit to the development of AuNRs as nanomaterials in theranostic applications. For example, photothermal therapy and photoacoustic imaging in human diseases will require particles with high absorbance cross sections for increased efficacy [54] and biosensors which require high scattering cross sections [24].

Acknowledgments

LR acknowledges the award of a PhD studentship through the University Research Scholarship by the University of Leeds. KC thanks the EPSRC for financial support (EP/P005233/1). SDE and PLC would like to thank the EPSRC (EP/P023266/1 and EP/P00122X/1) for financial support. The dataset associated with this paper is available from the University of Leeds: https://doi.org/10.5518/273.

ORCID iDs

Lucien Roach https://orcid.org/0000-0002-9166-6662

References

[1] Abadeer N S and Murphy C J 2016 *J. Phys. Chem.* C **120** 4691
[2] Austin L A, Mackey M A, Dreaden E C and El-Sayed M A 2014 *Arch. Toxicol.* **88** 1391
[3] Huang X and El-Sayed M A 2010 *J. Adv. Res.* **1** 1
[4] Jain S, Hirst D and O'Sullivan J 2012 *Br. J. Radiol.* **85** 101
[5] Jaque D, Martinez Maestro L, del Rosal B, Haro-Gonzalez P, Benayas A, Plaza J L, Martin Rodriguez E and Garcia Sole J 2014 *Nanoscale* **6** 9494
[6] Riley R and Day E 2017 *Wiley Interdiscip. Rev.: Nanomed. Nanobiotechnol.* **9** 1449
[7] Weber J, Beard P C and Bohndiek S E 2016 *Nat. Methods* **13** 639
[8] Aioub M, Panikkanvalappil S R and El-Sayed M A 2017 *ACS Nano* **11** 579
[9] Ali M R *et al* 2017 *Proc. Natl Acad. Sci.* **114** 3110
[10] Vankayala R, Lin C C, Kalluru P, Chiang C S and Hwang K C 2014 *Biomaterials* **35** 5527
[11] Wang L, Yuan Y, Lin S, Huang J, Dai J, Jiang Q, Cheng D and Shuai X 2016 *Biomaterials* **78** 40
[12] Ye S *et al* 2015 *Adv. Funct. Mater.* **25** 2117
[13] Pang B, Yang X and Xia Y 2016 *Nanomedicine* **11** 1715
[14] Brioude A, Jiang X and Pileni M 2005 *J. Phys. Chem.* B **109** 13138
[15] Yu Y Y, Chang S S, Lee C L and Wang C C 1997 *J. Phys. Chem.* B **101** 6661
[16] Park K, Biswas S, Kanel S, Nepal D and Vaia R A 2014 *J. Phys. Chem.* C **118** 5918
[17] Erickson T A and Tunnell J W 2007 *Gold Nanoshells in Biomedical Applications* (Weinheim: Wiley)
[18] Qin Z and Bischof J C 2012 *Chem. Soc. Rev.* **41** 1191
[19] Comenge J *et al* 2016 *ACS Nano* **10** 7106
[20] Shah A J, Alles E J, Box C, Eccles S A, Robinson S P, de Souza N and Bamber J C 2014 *Proc. SPIE* **8943** 89435G
[21] Huang X, El-Sayed I H, Qian W and El-Sayed M A 2006 *J. Am. Chem. Soc.* **128** 2115
[22] Choi W I, Kim J Y, Kang C, Byeon C C, Kim Y H and Tae G 2011 *ACS Nano* **5** 1995
[23] Heidari Z, Salouti M and Sariri R 2015 *Nanotechnology* **26** 195101
[24] Nusz G J, Curry A C, Marinakos S M, Wax A and Chilkoti A 2009 *ACS Nano* **3** 795
[25] Jana N R, Gearheart L and Murphy C J 2001 *Adv. Mater.* **13** 1389
[26] Canbek Z C *et al* 2015 *Cryst. Growth Des.* **15** 3637
[27] Sánchez-Iglesias A, Winckelmans N, Altantzis T, Bals S, Grzelczak M and Liz-Marzán L M 2017 *J. Am. Chem. Soc.* **139** 107
[28] Jana N 2005 *Small* **1** 875
[29] Ali M R K, Snyder B and El-Sayed M A 2012 *Langmuir* **28** 9807
[30] Liopo A, Wang S, Derry P J, Oraevsky A A and Zubarev E R 2015 *RSC Adv.* **5** 91587
[31] Scarabelli L, Grzelczak M and Liz-Marzán L M 2013 *Chem. Mater.* **25** 4232
[32] Vigderman L and Zubarev E R 2013 *Chem. Mater.* **25** 1450
[33] Wang W, Li J, Lan S, Rong L, Liu Y, Sheng Y, Zhang H and Yang B 2016 *Nanotechnology* **27** 165601
[34] Ye X *et al* 2012 *ACS Nano* **6** 2804
[35] Allen J M, Xu J, Blahove M, Canonico-May S A, Santaloci T J, Braselton M E, Blahove M and Stone J W 2017 *J. Colloid Interface Sci.* **505** 1172
[36] Nikoobakht B and El-Sayed M A 2003 *Chem. Mater.* **15** 1957
[37] Pallares R M, Su X, Lim S H and Thanh N T K 2016 *J. Mater. Chem.* C **4** 53
[38] Xu Y, Zhao Y, Chen L, Wang X, Sun J, Wu H, Bao F, Fan J and Zhang Q 2015 *Nanoscale* **7** 6790
[39] Ye X, Zheng C, Chen J, Gao Y and Murray C B 2013 *Nano Lett.* **13** 765
[40] Lai J, Zhang L, Niu W, Qi W, Zhao J, Liu Z, Zhang W and Xu G 2014 *Nanotechnology* **25** 125601
[41] Scarabelli L, Sánchez-Iglesias A, Pérez-Juste J and Liz-Marzán L M 2015 *J. Phys. Chem. Lett.* **6** 4270
[42] Khlebtsov B N, Khanadeev V A, Ye J, Sukhorukov G B and Khlebtsov N G 2014 *Langmuir* **30** 1696
[43] Xu N, Bai B, Tan Q and Jin G 2013 *Opt. Express* **21** 21639
[44] Prescott S and Mulvaney P 2006 *J. Appl. Phys.* **99** 123504
[45] Xu Z, Shen C, Cw X, Yang T, Chen S, Li H and Gao H 2006 *Chem. Phys. Lett.* **432** 222

[46] Wei Q, Jin J and Shen J 2008 *Nanosci. Nanotechnol.* **8** 5708
[47] Qin Z, Wang Y, Randrianalisoa J, Raeesi V, Chan W C, Lipiński W and Bischof J C 2016 *Sci. Rep.* **6** 29836
[48] Koshy P, Aswal V, Venkatesh M and Hassan P 2011 *J. Phys. Chem.* B **115** 10817
[49] El Kadi N, Martins F, Clausse D and Schulz P C 2003 *Colloid Polym. Sci.* **281** 353
[50] Miraglia D B, Rodríguez J L, Minardi R M and Schulz P C 2010 *J. Surfactants Detergents* **14** 401
[51] Javadian S, Ruhi V, Heydari A, Asadzadeh Shahir A, Yousefi A and Akbari J 2013 *Ind. Eng. Chem. Res.* **52** 4517
[52] Kunz W, Testard F and Zemb T 2008 *Langmuir* **25** 112
[53] Gans R 1912 *Ann. Phys.* **342** 881
[54] Mackey M A, Ali M R K, Austin L A, Near R D and El-Sayed M A 2014 *J. Phys. Chem.* B **118** 1319